The decadal variability of the tropical Indian Ocean SST–the South Asian High relation: CMIP5 model study

X. Qu & G. Huang

Climate Dynamics
Observational, Theoretical and Computational Research on the Climate System

ISSN 0930-7575
Volume 45
Combined 1-2

Clim Dyn (2015) 45:273-289
DOI 10.1007/s00382-014-2285-3

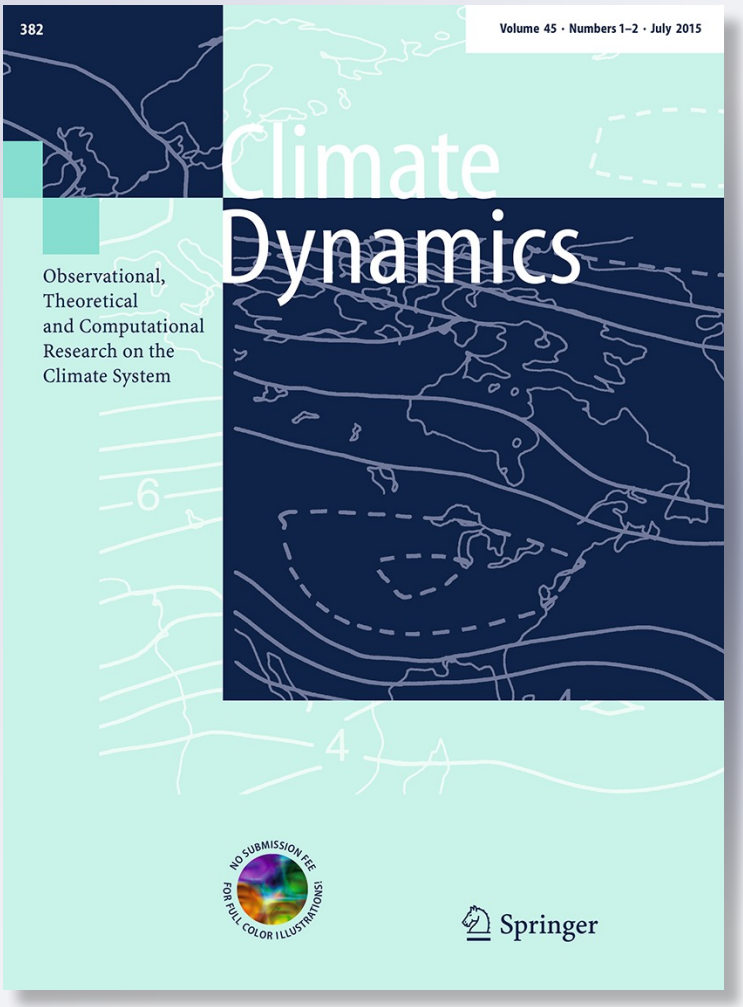

Springer

Clim Dyn (2015) 45:273–289
DOI 10.1007/s00382-014-2285-3

The decadal variability of the tropical Indian Ocean SST–the South Asian High relation: CMIP5 model study

X. Qu · G. Huang

Received: 10 March 2014 / Accepted: 1 August 2014 / Published online: 19 August 2014

Abstract Based on Coupled Model Intercomparison Project phase 5 (CMIP5) models, present study investigates the decadal variability of the tropical Indian Ocean (TIO) sea surface temperature (SST)–the South Asian High (SAH) relation (hereafter TSR) as well as its responses to the global warming. Out of the 17 CMIP5 models, only one (GFDL-CM3) reproduces reasonably the influence of the TIO SST on the SAH. In the historical simulations of GFDL-CM3, the TSR features fluctuations modulated by the western Pacific SST and the Indian subcontinent precipitation. When the TIO warming is accompanied by warm western Pacific, the western Pacific SST-induced tropospheric warming propagates westwards, warms the troposphere surrounding the Indian Ocean, enhances SAH and leads to higher TSR; when accompanied by not so warmed western Pacific, the TSR is lower. While, if the TIO warming is accompanied by negative rainfall anomalies over the Indian subcontinent, the rainfall-induced upper-troposphere cyclone over the subtropical Asia weakens the response of the SAH and leads to lower TSR; if not accompanied by negative rainfall anomalies, the TSR is higher. The decadal variability of the TSR is not subject to the global warming. In RCP45 and RCP85 scenarios, the TSR is also not directly affected by global warming. The rainfall over the Indian subcontinent is still a factor modulating the TSR. While, the western Pacific SST is invalid in the influences of the TIO SST on the SAH.

Keywords The tropical Indian Ocean · The South Asian High · Tropospheric temperature · Decadal variability

1 Introduction

In boreal summer, a high pressure system, called the South Asia High (SAH) or the South Asian Anticyclone, lies in the upper troposphere over the Tibetan Plateau and the surrounding area. It is the strongest and steadiest system in the upper troposphere (Mason and Anderson 1963; Li et al. 2005). Two causes mainly account for the formation of the SAH. One is the elevated heating of the Tibetan Plateau. In boreal summer, the Tibetan Plateau is a huge elevated heating source, which excites anticyclone in the upper troposphere (Duan and Wu 2005). The other cause is the South Asian monsoon rainfall. Using conceptional models, Hoskins and Rodwell (1995) and Qu et al. (2014) suggested that the latent heating associated with the South Asian monsoon rainfall also forms the anticyclonic circulation in the upper troposphere over the subtropical Asia.

East Asia is one of the most highly populated regions. Severe floods and droughts, induced by the strong interannual variability of the East Asia summer monsoon (Huang

X. Qu
Center for Monsoon System Research, Institute of Atmospheric Physics, Chinese Academy of Sciences, Beijing 100029, China

X. Qu
Key Laboratory of Meteorological Disaster, Nanjing University of Information Science and Technology, Ministry of Education, Nanjing 210044, China

G. Huang (✉)
Key Laboratory of Regional Climate-Environment Research for Temperate East Asia, Institute of Atmospheric Physics, Chinese Academy of Sciences, P. O. Box 9804, Beijing 100029, China
e-mail: hg@mail.iap.ac.cn

G. Huang
Collaborative Innovation Center on Forecast and Evaluation of Meteorological Disasters, Nanjing University of Information Science and Technology, Nanjing 210044, China

et al. 1999), exert great societal and economic influence. The East Asian summer monsoon rainfall is closely linked to the western Pacific subtropical high (Tao and Chen 1987; Huang and Wu 1989; Huang and Sun 1992; Wu and Chen 1998). The variation of the subtropical high follows that of the SAH (Tao and Zhu 1964; Jiang et al. 2011). On interannual timescale, the intensified SAH, through emanating anomalous wave energy downstream, strengthens the subtropical high (Zhao et al. 2009). Consequently, the rainfall decreases over the northwestern Pacific and increases over East Asia (Zhao et al. 2007; Zhang et al. 2005). In addition, studies suggested that the interannual variability of the SAH is associated with the South Asia monsoon, the mid-Pacific trough, and the Mexico high (Zhang et al. 2005; Zhao et al. 2007).

The interannual variability of the SAH is shown to relate to the tropical Indian Ocean (TIO) sea surface temperature (SST) (Zhang et al. 2000; Yang et al. 2007; Huang et al. 2011). On interannual timescale, the TIO basin warms up after the peak of El Niño events through "atmospheric bridge" and oceanic dynamics (Du et al. 2009; Klein et al. 1999; Xie et al. 2002). This warming persists to summer when El Niño has dissipated and exerts influences on climate (Annamalai et al. 2005; Yang et al. 2007; Xie et al. 2009). The persistent warming in summer, through convection and moist adjustment, heats the local troposphere column, forces the Kelvin wave to the east and affects the western North Pacific climate (Xie et al. 2009; Chowdary et al. 2011) as well as the East Asia climate (Hu et al. 2011, 2012). The warmed troposphere over the TIO corresponds to an elevated geopotential in the upper troposphere and leads to intensified SAH (Huang et al. 2011). The effect of the TIO on the SAH experienced intensification around the late-1970s (Qu and Huang 2012).

Greenhouse gases in the atmosphere have been increasing since the Industrial Revolution, contributing to a rise in global surface temperature. Nevertheless, the rise is spatially uneven due to many factors, such as the diverse property of the earth surface (the small heat content of land and evaporation of the ocean; Sutton et al. 2007), the ice/snow albedo feedback (Manabe et al. 1990) and polarward energy transport (Cai 2005). This tends to cause an inhomogeneous response in the atmosphere (Xie et al. 2010a). The influences of the increasing greenhouse gases on climate are sophisticated. It is not understood how the effects of the TIO on the SAH behave under such a gradually warming climate or projected warmer scenario.

General circulation models provide the possibility to look into the problem. Coupled Model Intercomparison Project (CMIP) phase 3 models are capable to reproduce the SAH (Zhou et al. 2006, 2009). Besides, Du et al. (2013) evaluated the CMIP phase 5 (CMIP5) models and showed that the models have the ability to capture the oceanic/atmospheric process associated with the Indian Ocean basin warming (IOBM). However, the relationship between SAH and TIO SST is not been studied using CMIP5 in both historical and global warming. The present study aims to address the above problems using the CMIP5 models.

Table 1 Information of the climate models

Model ID	Ensemble member (historical)	Ensemble member (RCP45)	Ensemble member (RCP85)	Atmospheric resolution
CanESM2	1, 2, 3			128 × 64
CNRM-CM5	1, 2, 3			256 × 128
CSIRO-Mk3-6-0	1, 2			192 × 96
FGOALS-s2	1, 2, 3			128 × 96
GFDL-CM3	1, 2	1	1	144 × 90
GFDL-ESM2G	1			144 × 90
GISS-E2-R	1, 2,			144 × 90
HadGEM2-CC	1			192 × 145
HadGEM2-ES	1			192 × 145
inmcm4	1			180 × 120
IPSL-CM5A-LR	1, 2, 3			96 × 96
MIROC-ESM	1, 2			128 × 64
MIROC-ESM-CHEM	1			128 × 64
MIROC5	1, 2, 3			256 × 224
MPI-ESM-LR	1, 2, 3			192 × 96
MRI-CGCM3	1, 2, 3			320 × 160
NorESM1-M	1			144 × 96

From http://cmip-pcmdi.llnl.gov/cmip5/docs/CMIP5_modeling_groups.pdf

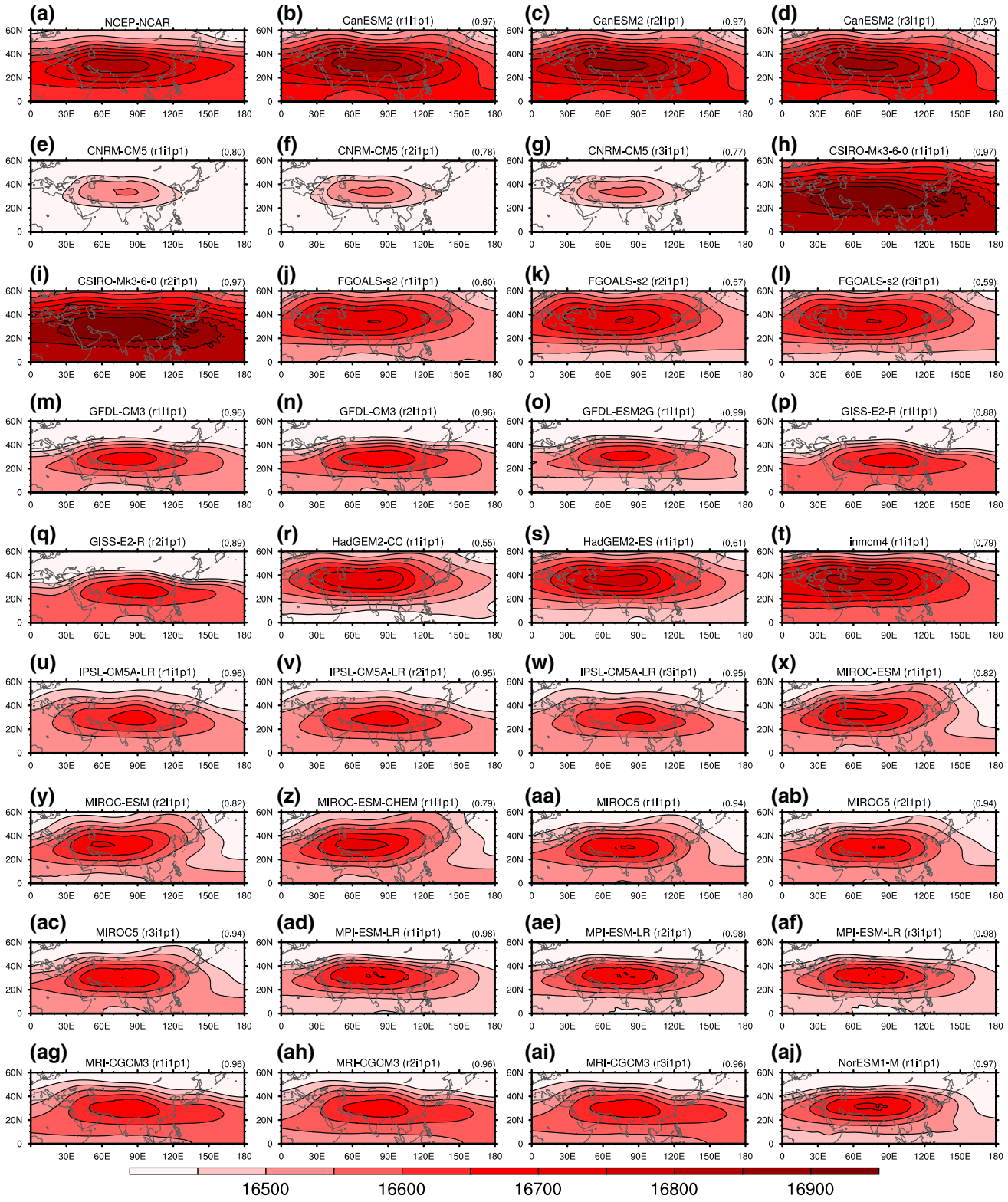

Fig. 1 Summer mean 100 hPa geopotential height for 1979–2005. *Topleft* is the result of NCEP–NCAR reanalysis and the rest are the results of CMIP5 simulations (the model ID are on the *top* of *each figure*, the corresponding ensemble names are in *parentheses*). The pattern correlation coefficients with the NCEP–NCAR reanalysis over the domain are shown at the *top-right* corners of each figure. The units are m

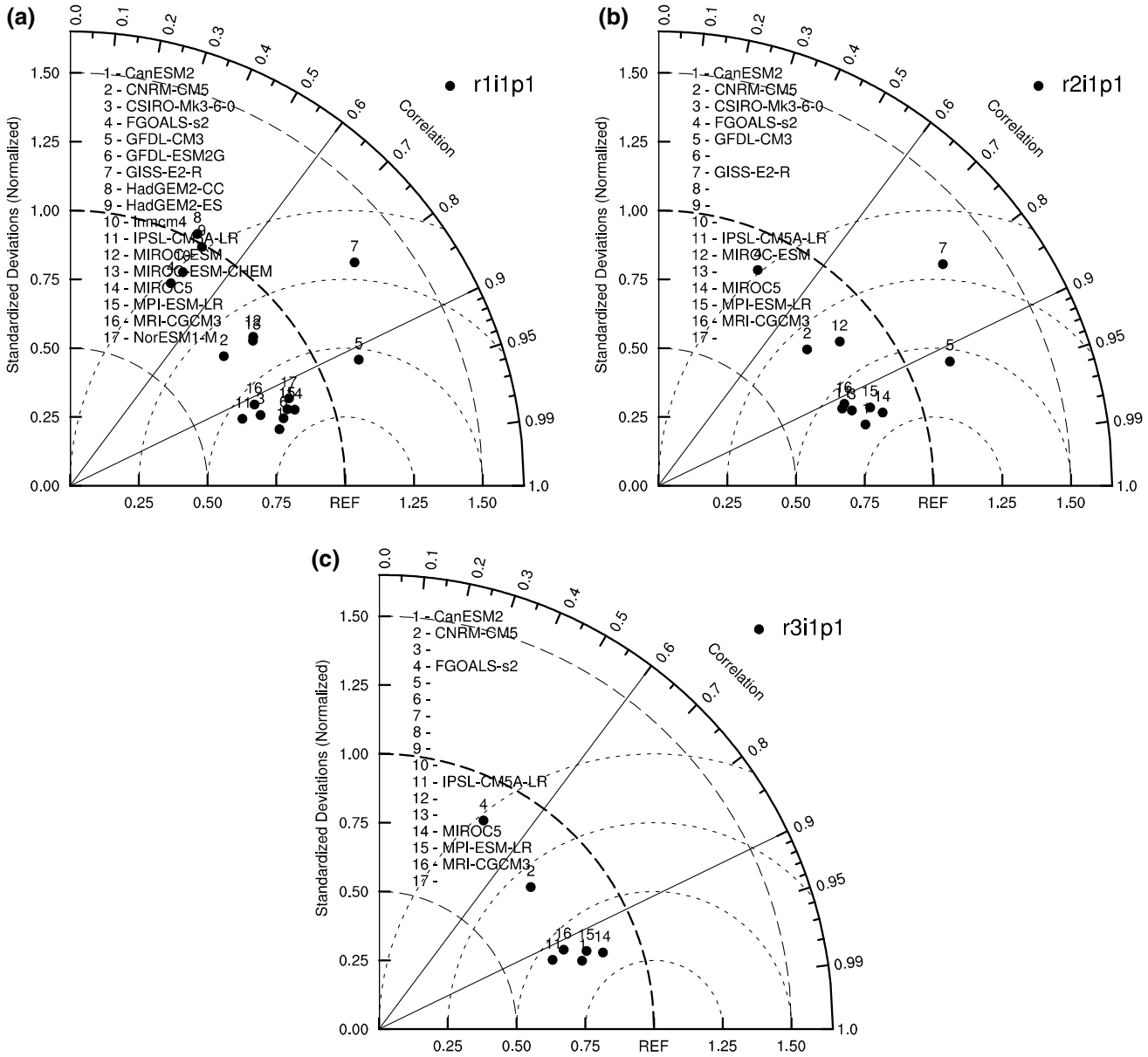

Fig. 2 The taylor diagram of geopotential height at 100 hPa over the [15–45°N; 10–140°E]. **a–c** The results of r1i1p1, r2i1p1 and r3i1p1, respectively. The pattern correlation with the climatological pattern of the 100 hPa geopotential height based on NCEP–NCAR reanalysis over the domain is shown as the azimuthal position, while the radial distance indicates the standard deviation of the pattern of the 100 hPa geopotential height normalized by that based on NCEP–NCAR reanalysis

The paper is organized as follows: Sect. 2 introduces data and methods; Sect. 3 evaluates the performance of the CMIP5 models in simulating the SAH and its association with the Indo-Pacific SST, mainly the TIO SST; Sect. 4 explores the factors modulating the TIO SST–SAH relation (TSR) from 1860 to 2005 in historical simulation; Sect. 5 investigates the decadal variability of the TSR and corresponding factors in warmer climate (the RCP45 and RCP85 runs); Sect. 6 summarizes the results.

2 Data and methods

This investigation is based on CMIP5 model outputs. The information for the CMIP5 models is listed in Table 1. The experiments analyzed in this study are historical, RCP45 and RCP85 simulations. The historical experiments were conducted based on observed anthropogenic and natural forcing from the mid-nineteenth century to 2005. In the RCP45 and RCP85 experiments, the CMIP5 models were forced by gradual increased radiative forcing

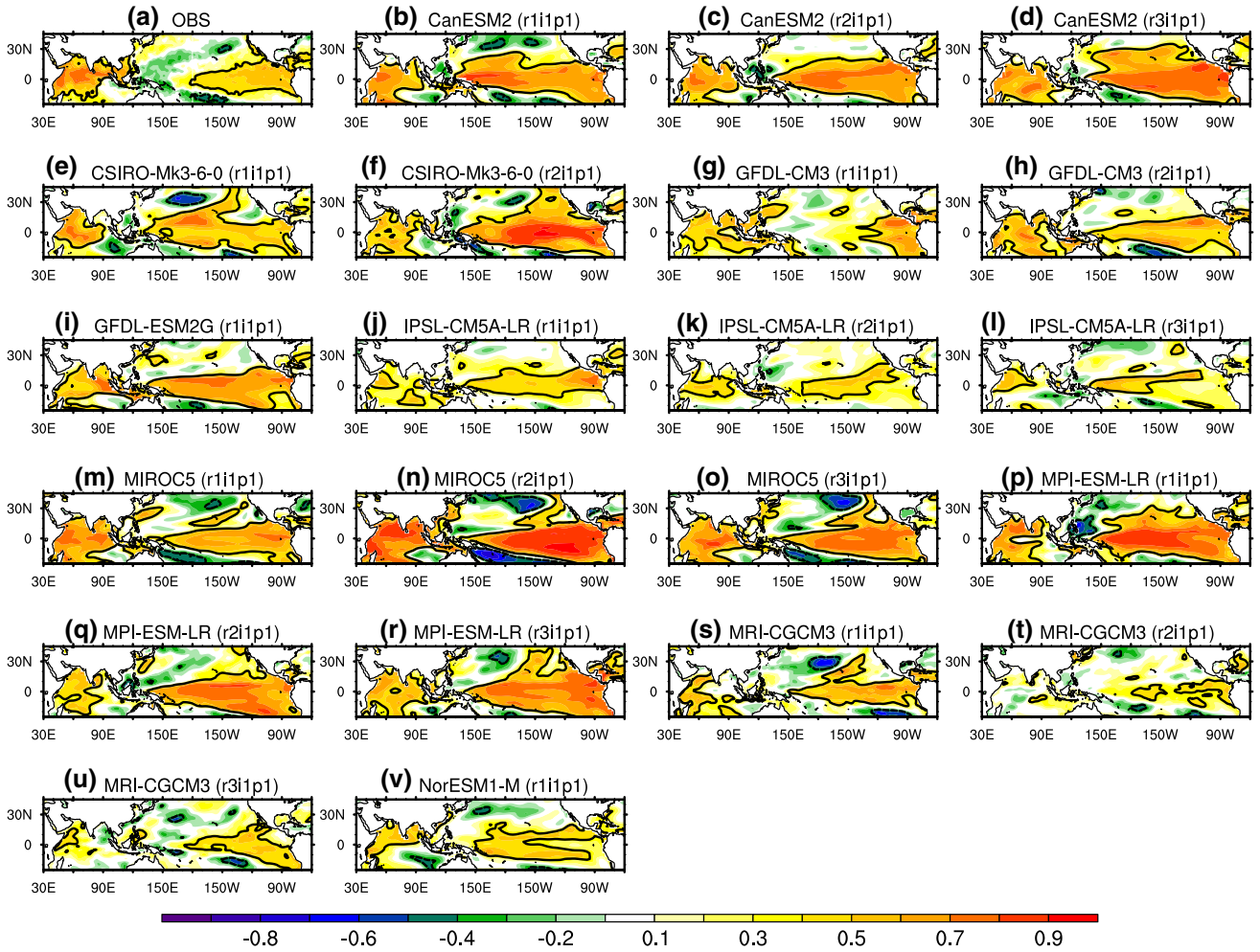

Fig. 3 The correlation of normalized SAH intensity with the SST in preceding winter (N(0)D(0)J) during 1980–2005. The *solid* and *dash contours* denote the correlation coefficients 0.388 and −0.388, respectively. **a** NCEP–NCAR reanalysis and HadISST result, while **b–v** the CMIP5 model results (the model ID are on the *top* of *each figure*, the corresponding ensemble names are in *parentheses*). The numeral "0" denote the preceding year

which stabilizes at 4.5 W m^{-2} in RCP45 and 8.5 W m^{-2} in RCP85 after 2100 (Riahi et al. 2011; Thomson et al. 2011). For detailed information, readers are referred to the following web site: http://cmip-pcmdi.llnl.gov/cmip5/. The ensemble members used in present study are list in Table 1. The analysis is focused on summer (i.e., June–July–August) mean. The performances of CMIP5 models are evaluated against: (1) the National Centers for Environmental Prediction–National Center for Atmosphere Research (NCEP–NCAR) atmospheric reanalysis with a horizontal resolution of 2.5° × 2.5° (Kalnay et al. 1996); and (2) the Hadley Center Global Sea Surface Temperature (HadISST) dataset with a horizontal resolution of 1.0° × 1.0° (Rayner et al. 2006). For convenience, the observational dataset and reanalysis are all called "observations".

The present study focuses the interannual variability and its decadal change. Since long time variability is significant in both the Indo-Pacific SST and the SAH (Zhang et al. 2000; Du and Xie 2008), the data have been detrended to eliminate the contribution of trends to the statistical results. Unless stated, the detrending is performed on the data of each target period, respectively. For instance, if the target period of analysis is from 1980 to 2005, the trend for this period is removed before the analysis.

3 Present-day climate

In this section, the behaviors of the climatological pattern of the SAH and the influence of the Indo-Pacific SST (mainly the TIO SST) on the SAH in the CMIP5 models are examined.

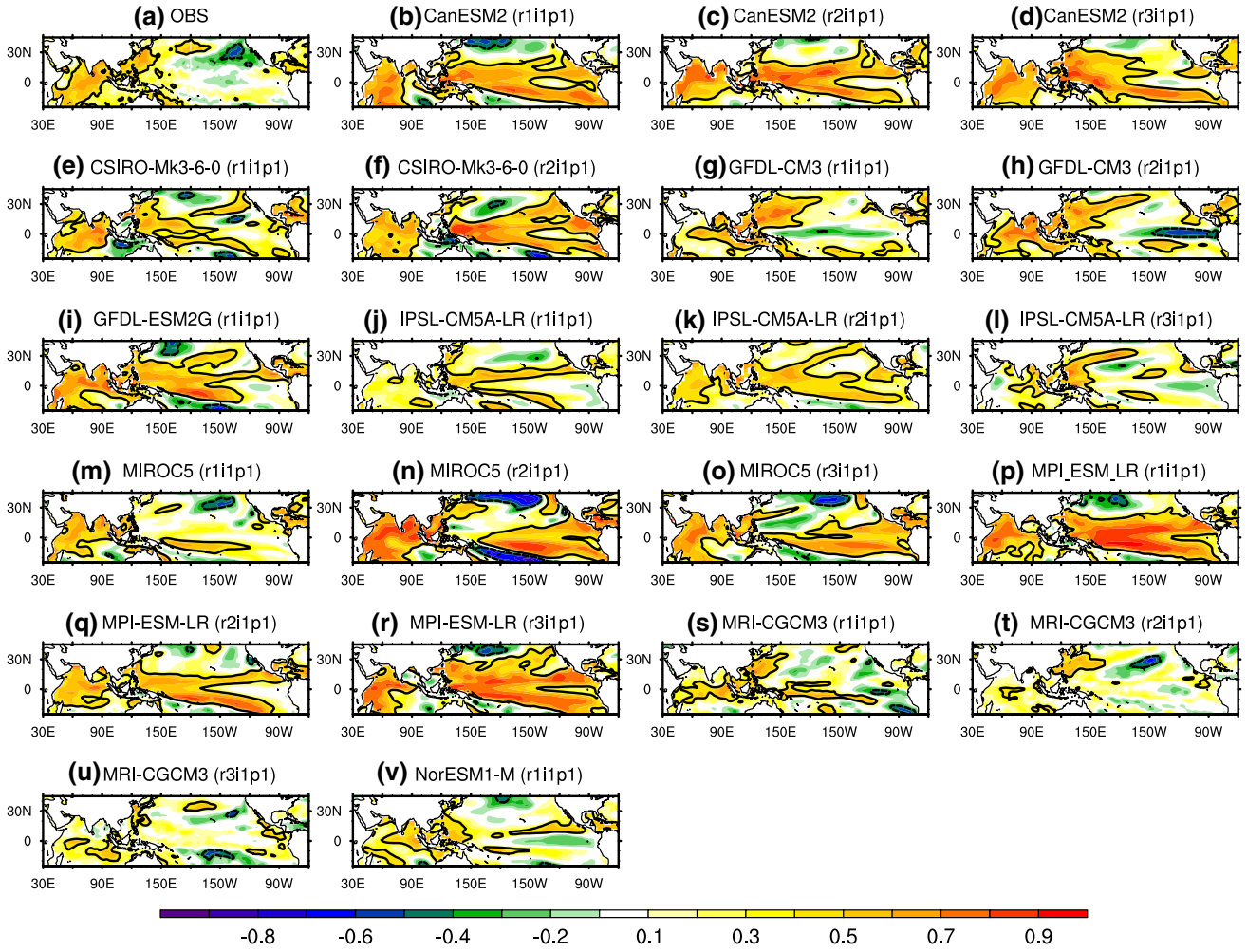

Fig. 4 The same as Fig. 3, except for JJA SST

3.1 The SAH climatology

First, the climatological pattern of the SAH is evaluated. Figure 1 displays the summer mean 100 hPa geopotential height for 1979–2005 in NCEP–NCAR reanalysis and the CMIP5 models. In NCEP–NCAR reanalysis, at 100 hPa, the SAH features a zonally elongated ellipse, with centers over the Tibetan Plateau and the Iran Plateau (Fig. 1a). Most CMIP5 models reasonably simulate the high. Based on the similarity of the spatial pattern, CanESM2 shows the best skill, with a pattern correlation coefficient of approximate 0.96; CNRM-CM5, FGOALS-s2, GISS-E2-R, HadGEM2-CC, HadGEM2-ES, inmcm4, MIROC-ESM and MIROC-ESM-CHEM exhibit lower skill; the similarities in the rest models are reasonable (Fig. 2). The models that reproduce better the pattern of the thermal contrast, defined by the thickness between 100 hPa and 500 hPa, tend to yield better the SAH (figures not shown). Based on the standard deviation of the climatological pattern of 100 hPa geopotential height over [15–45°N; 10–140°E], HadGEM2-CC and HadGEM2-ES are close to observation; GFDL-CM3 and GISS-E2-R simulate higher standard deviation, while the rest yield lower standard deviation (Fig. 2). The distances to the reference point at x-axis in Fig. 2 denote the root-mean-square differences between simulations and observation. CanESM2, CSIRO-Mk-3-6-0, GFDL-CM3, GFDL-ESM2G, IPSL-CM5A-LR, MIROC5, MPI-EMS-LR, MRI-CGCM3 and NorESM1-M exhibit relatively reasonable root-mean-square differences. For clarity, the other models are excluded for the following analysis.

3.2 Influence of the Indo-Pacific SST on the SAH

In observation, the interannual variability of the SAH is subjected to the influence of IOBM following El Niño in

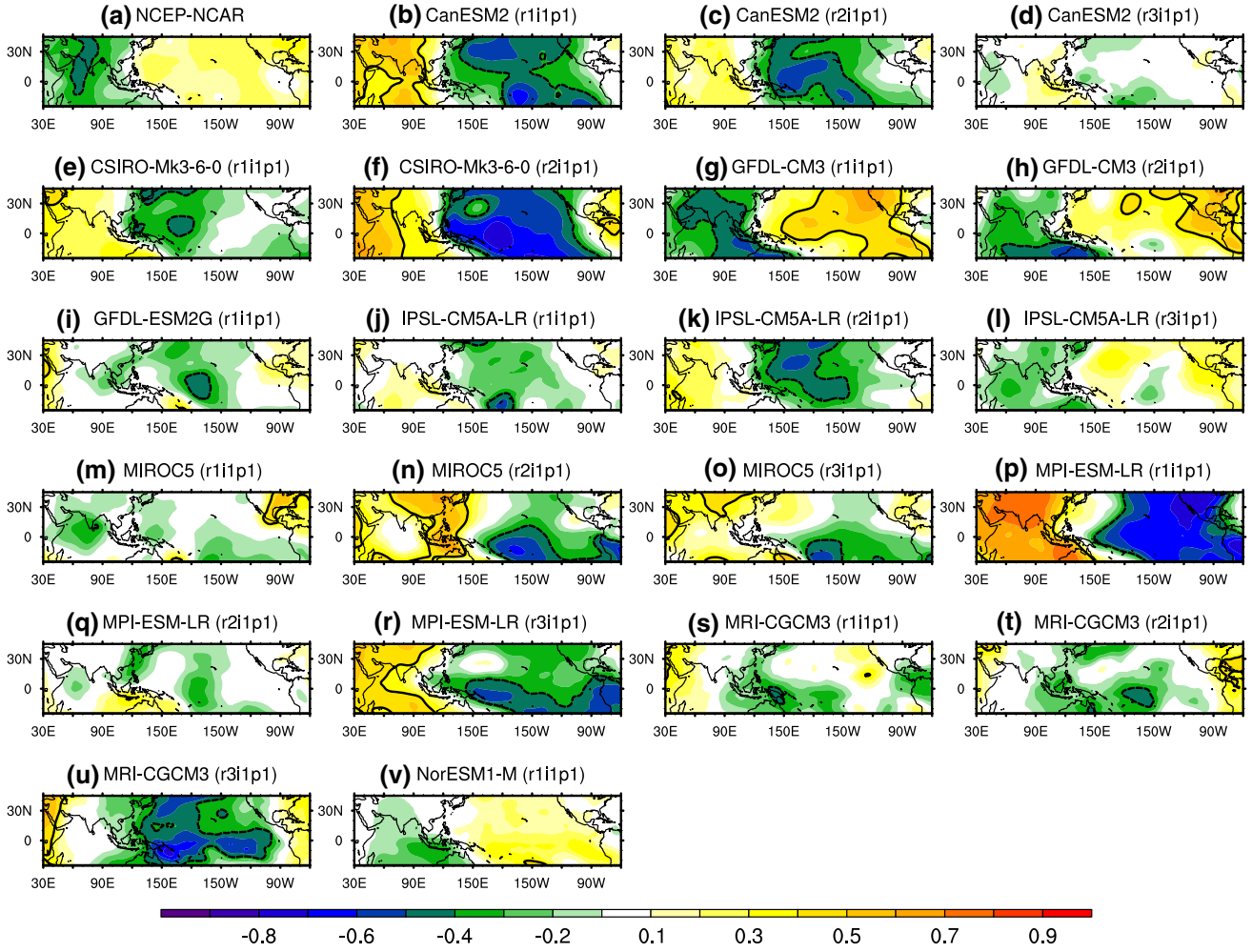

Fig. 5 The same as Fig. 4, except for JJA velocity potential at 200 hPa

preceding winter after the late-1970s (Huang et al. 2011; Qu and Huang 2012; Yang et al. 2007; Zhang et al. 2000). Here, we evaluate the relation between the SAH and the Indo-Pacific SST (mainly the TIO SST) in CMIP5 model simulations. The TIO SST is defined as the regional averaged SST over the domain [20°S–20°N; 40°E–100°E] with latitudinal weight; the SAH is defined as geopotential height averaged over the domain [15°N–45°N; 10°E–140°E].

Most of the CMIP5 models are capable of reproducing the SST anomalies during the preceding winter in the years when the SAH is intensified. During the preceding winter, significant warming exists over the eastern Pacific and the TIO basin in observation (Fig. 3a). The IOBM arises from El Niño-induced cloud and shortwave radiation change and ocean waves (Klein et al. 1999; Xie et al. 2002). All the CMIP5 models are able to reproduce the previous ENSO, except that NorESM1-M do not show reasonable SST anomaly pattern in the eastern Pacific; several ensembles do not well reproduce the ENSO pattern, such as r1i1p1 of GFDL-CM3, r2i1p1 and r3i1p1 of IPSL-CM5A-LR and r2i1p1 of MRI-CGCM3 (Fig. 3b–v). The CMIP5 models generally exaggerate the ENSO–SAH relation. The IOBM during the winter is simulated in most of the CMIP5 models except for IPSL-CM5A-LR (r1i1p1, r2i1p1 and r3i1p1) and MRI-CGCM3 (r1i1p1, r2i1p1 and r3i1p1) (Fig. 3b–v). In the models capable of reproducing El Niño, the warming extends unexceptionally far westwards. This may be due to the westward extension bias of the Pacific cold tongue in the climate models (Li and Xie 2014; Du et al. 2013).

Quite few CMIP5 models can reproduce the simultaneous SST features associated with the year-to-year variability of the SAH. During the summer following El Niño, apparent SST anomalies dissipate over the eastern Pacific,

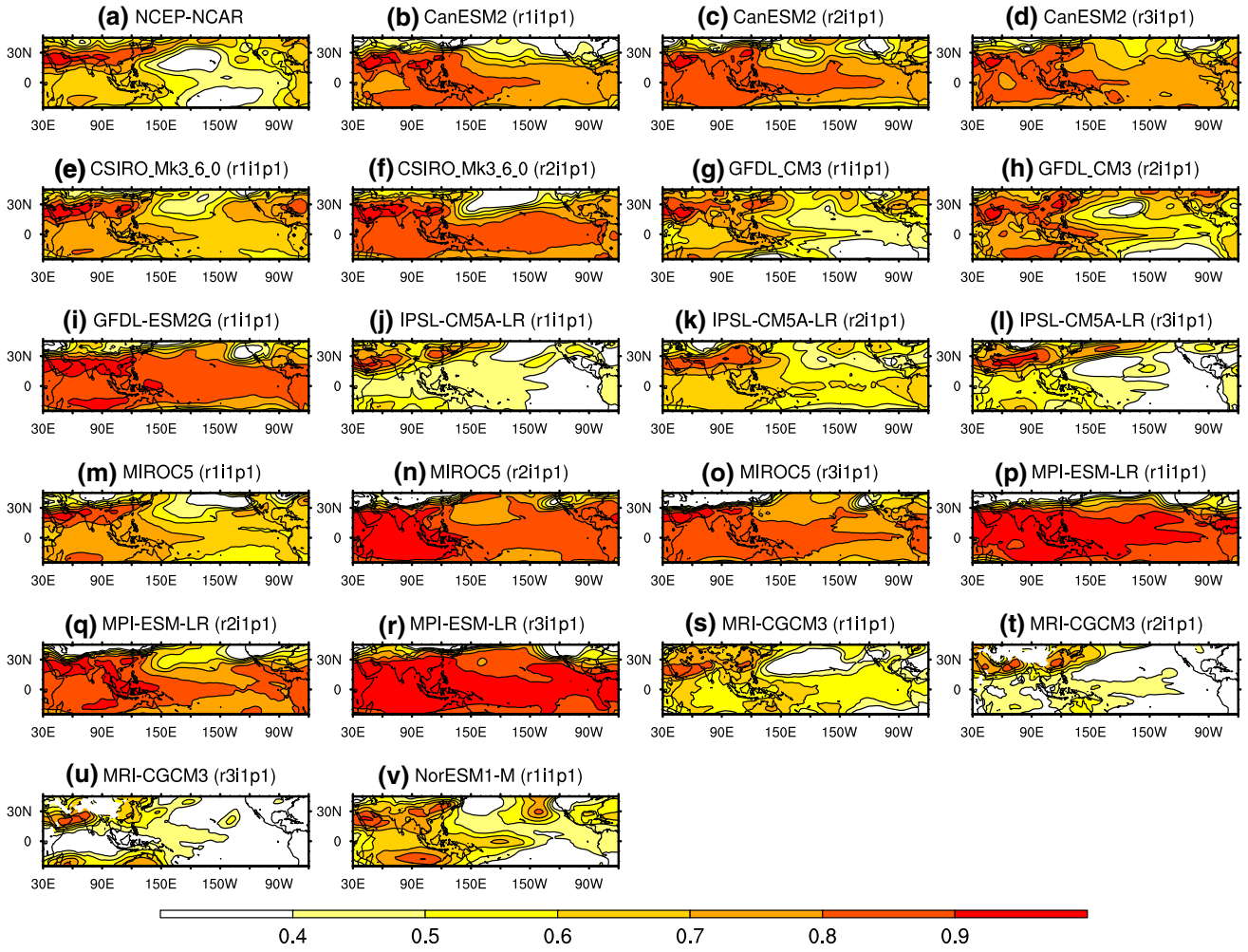

Fig. 6 The simultaneous correlation of normalized SAH intensity with the tropospheric temperature during 1980–2005. **a** The NCEP–NCAR reanalysis result, while **b**–**v** the CMIP5 model results (the model ID are on the *top* of *each figure*, the corresponding ensemble names are in *parentheses*)

and significant warming exists over the TIO (Fig. 4a). Most models are able to reproduce the IOBM except for MRI-CGCM3 and NorESM1-M; several ensembles of the models do not well simulate the basin warming, such as r1i1p1 of GFDL-CM3, r1i1p1 and r3i1p1 of IPSL-CM5A-LR (Fig. 4b–v). Most ensembles fail to reproduce the SST anomalies over the Pacific. All the ensembles in CanESM2, CSIRO-Mk3-6-0, GFDL-ESM2G and MPI-ESM-LR, as well as r1i1p1 and r2i1p1 of IPSL-CM5A-LR and r2i1p1 and r3i1p1 of MIROC5, exhibit significant warming over the Pacific. All the ensembles of GFDL-CM3, MRI-CGCM3 and NorESM1-M display relatively reasonable SST anomalies over the Pacific.

Figure 5 displays the correlation of the SAH intensity with the simultaneous velocity potential at 200 hPa during 1980–1995. In the observations, if the SAH intensified, negative velocity potential anomaly exists over the Indian Ocean, while positive anomaly over the Pacific (Fig. 5a), indicating the dominance of the TIO SST over the tropical Pacific. Among the CMIP5 models, all the ensembles of GFDL-CM3 and NorESM1-M, as well as the r3i1p1 of IPSL-CM5A-LR, are able to reasonably reproduce the velocity potential pattern in the upper troposphere; the others fail to reproduce the large-scale pattern (Fig. 5b–v).

The associated tropospheric temperature response is reasonably reproduced in most of the models. The tropospheric temperature, defined as mean temperature between 100 and 850 hPa, acts as a medium in the influence of the Indian Ocean SST on the SAH. In tropical atmosphere, the temperature approximately follows the moist adiabatic profile, determined by equivalent potential temperature in the planetary boundary layer (Emanuel et al. 1994, 1997). As

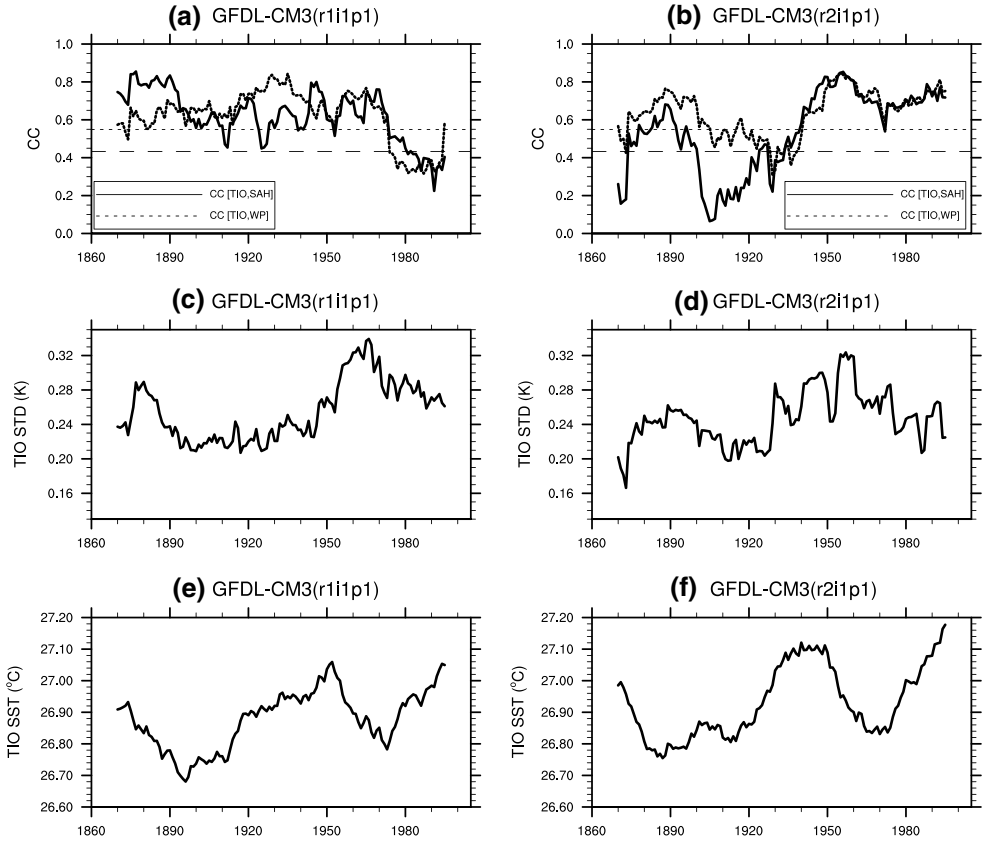

Fig. 7 **a**, **b** The 21-year sliding correlation coefficient between the TIO SST and the SAH (*black solid line*) and correlation coefficient between the TIO SST and the western Pacific [20°S–20°N; 120°–180°E] SST (*black dash line*). The 21-year sliding standard deviation (**c**, **d**) and average (**e**, **f**) of the TIO SST. The *long* (*short*) *thin dash lines* in **a** and **b** mean the correlation reaching 95 % (99 %) significance level. The results are based on GFDL-CM3 historical run. **a**, **c**, **e** The results of r1i1p1; **b**, **d**, **f** the results of r2i1p1

the TIO basin warms in the summer following El Niño, the surface equivalent potential temperature increases, the whole troposphere column warms, forcing Kelvin wave response to the east of the Indian Ocean, like a wedge penetrating into the equatorial Pacific (Xie et al. 2009); the tropospheric warming above the TIO basin leads to elevated height over South Asia and thus the enhanced SAH (Huang et al. 2011). It is evident in Fig. 6a. Out of the CMIP5 models, only one model (MRI-CGCM3) does not reasonably reproduce IOBM-induced Kelvin wave response (Fig. 6b–v). In NorESM1-M, despite resemblances of the Kelvin wave and tropospheric temperature response over the TIO to the observation (Fig. 6v), the underlying basin warming is not clear (Fig. 4v); the response may not be the impacts of IOBM. The CMIP5 models generally overestimate the tropospheric temperature response, which may result from the exaggerated tropospheric temperature–SST relation in the models (figures not shown).

Based on the above results, the r2i1p1 of GFDL-CM3 most reasonably reproduces and the climatology of the SAH and the anomalous features associated with the enhancement of the SAH during 1980–2005, including the preceding El Niño and simultaneous evanishment of El Niño, below normal velocity potential, tropospheric warming over the Indian Ocean. Therefore, GFDL-CM3 is capable to reproduce the relevant features of the SAH and IOBM and is proper to study the TSR.

4 Decadal change in the influences

Owing to ENSO and the Southwestern Indian Ocean thermocline change, the influences of the Indian Ocean SST on systems in the surrounding regions, including the SAH, are intensified around the late 1970s (Huang et al. 2010; Qu and Huang 2012; Xie et al. 2010b). Does the accompanied global warming modulate the decadal change of the influence? In this section, we aim to address this question.

Our analyses suggested that global warming does not directly affect the decadal change of the TSR, in the past

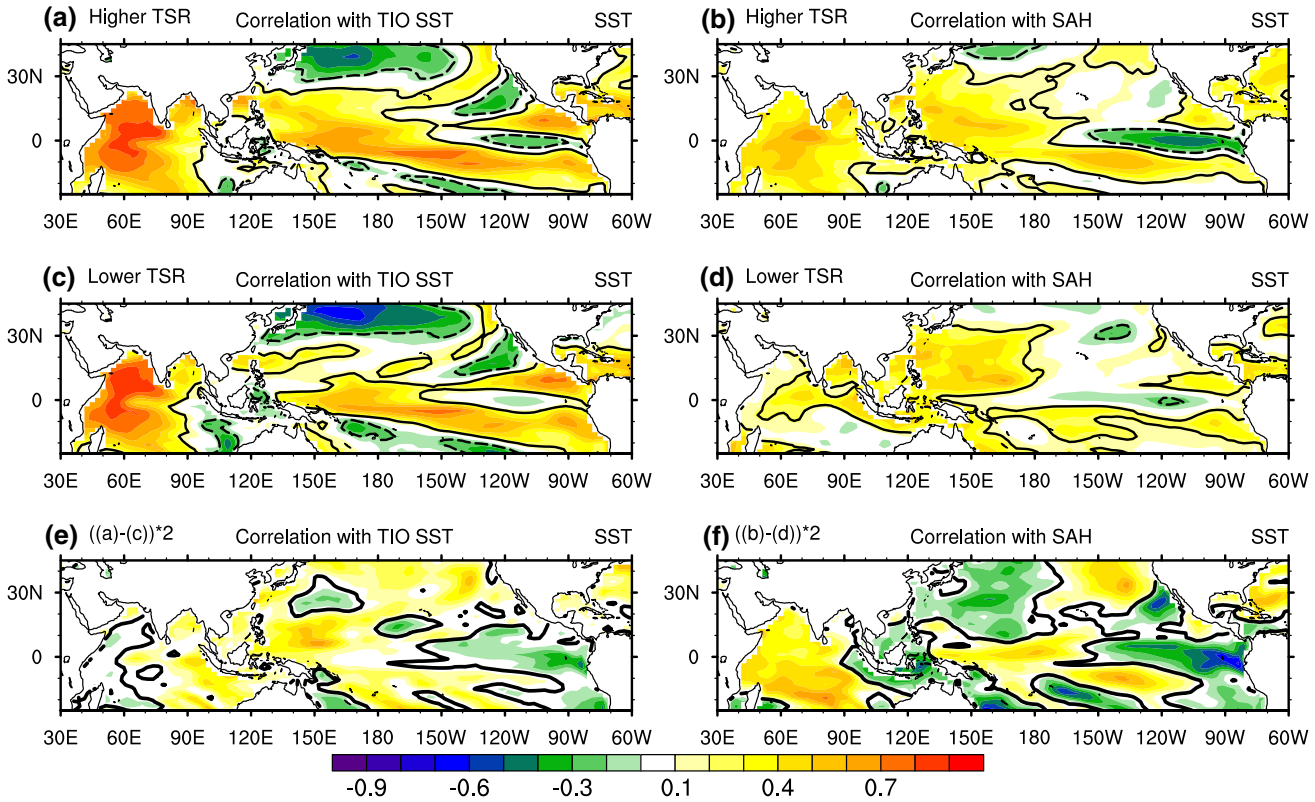

Fig. 8 The correlation of the TIO SST index (**a**, **c**) and SAH (**b**, **d**) with the JJA Indo-Pacific SST in GFDL-CM3 historical run. **a**, **b** The results during TSR is higher; **c**, **d** the results during TSR is lower. **e** 2 times the result of **a** minus **c**. **f** 2 times the result of **b** minus **d**. *Solid* (*dash*) *contours* in **a**–**d** mean the positive (negative) results reaching 95 % significance level. *Solid contours*in **e** and **f** mean the results are zero. The results are based on the combination of r1i1p1 and r2i1p1. A 9-year running average has been used to remove longer variation of the raw data. Spatial 9-point smooth is performed for clarity

Table 2 The corresponding years of higher and lower cases in each ensembles of GFDL-CM3 in historical simulation

Simulations	Ensemble	Case (number)	Years
Historical	r1i1p1	Higher cases (30)	1870, 1871, 1875–1893, 1944–1948, 1965, 1966, 1969, 1970
		Lower cases (30)	1911, 1912, 1924–1927, 1939, 1953, 1974–1995
	r2i1p1	Higher cases (31)[a]	1944–1963, 1966, 1982, 1983, 1987–1991, 1993–1995
		Lower cases (30)	1870–1873, 1901–1923, 1928–1932
RCP45	r1i1p1	Higher cases (30)	2053–2065, 2067–2074, 2077–2087
		Lower cases (30)	2016–2030, 2035–2045, 2049, 2050, 2089, 2090
RCP85	r1i1p1	Higher cases (30)	2016–2025, 2030–2033, 2035–2038, 2078–2090
		Lower cases (30)	2026–2028, 2040–2044, 2048–2057, 2059, 2060, 2064–2070, 2075–2077

[a] The 31 cases are selected for it equals the 30th of the 21-year sliding TSR in descent order

about 150 years. Figure 7 shows the 21-year sliding correlation coefficient between the TIO SST and the SAH in GFDL-CM3. In r1i1p1, the TSR gradually weakens from the late-nineteenth century to the end of historical simulation, opposite to global warming trend. However, in r2i1p1, the TSR generally displays positive trend. The TSR in the two ensembles show different relation with global warming. It implies that the TSR fluctuation may not be directly modulated by global warming, but is likely due to internal variability. The result is similar to the decadal variability of ENSO-TIO climate in Chowdary et al. (2012).

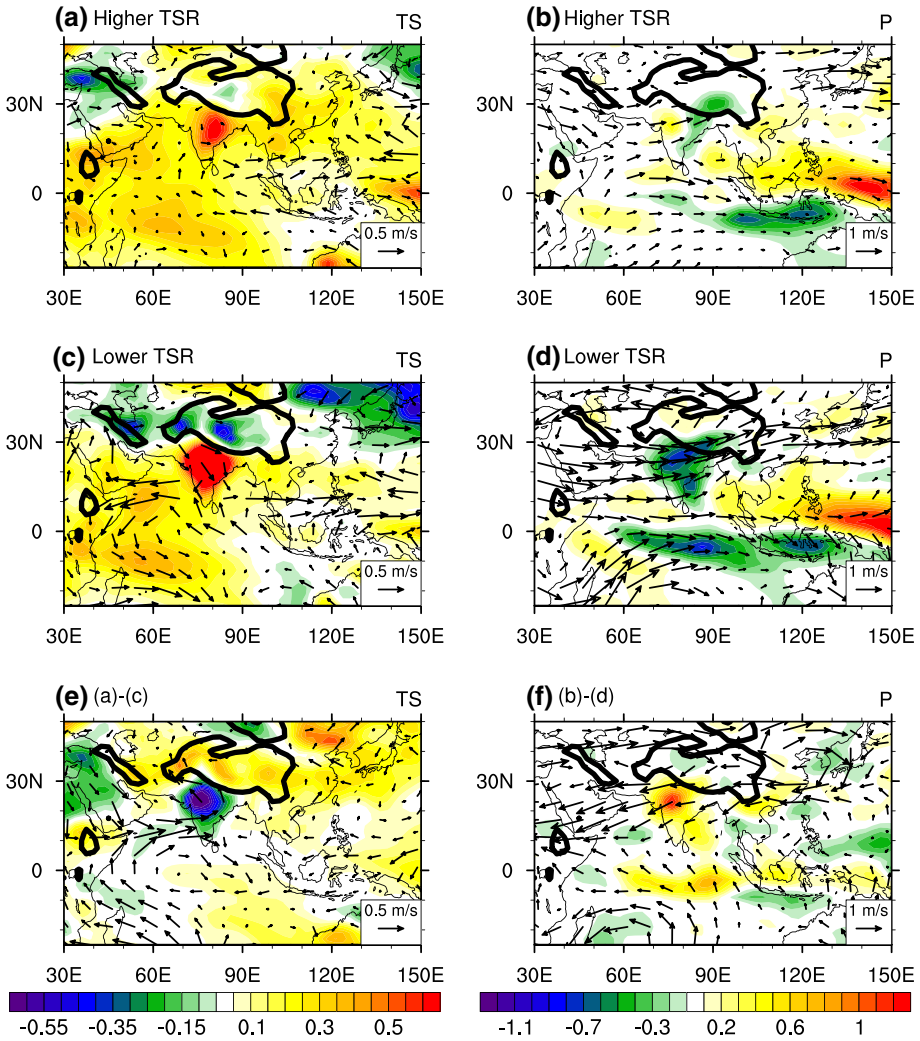

Fig. 9 The regression of the normalized TIO SST index in GFDL-CM3 historical run against: (1) surface temperature (unit: K) and 850 hPa wind (**a**, **c**, **e**); (2) precipitation (unit: mm/day) and 200 hPa wind (**b**, **d**, **f**). **a**, **b** The results of higher cases; **c**, **d** the results of lower cases. **e** The result of **a** minus **c**. **f** The result of **b** minus **d**. *Thick contours* denote the elevation is 1,500 m. The results are based on the combination of r1i1p1 and r2i1p1. A 9-year running average has been used to remove longer variation of the raw data. Spatial 9-point smooth is performed for clarity

The explanations to the observed change of the TIO influence in late 1970s cannot be applied to the decadal variability in the whole historical results of the model. Qu and Huang (2012) addressed the TIO influence change on SAH in the late 1970s using the NCEP–NCAR reanalysis and HadISST, and proposed two possible causes to the enhanced influence: (1) enhanced variability with higher climatological SST over the TIO; (2) significant warming within the warmpool when TIO warms. Correspondingly, the TIO SST feature is studied in GFDL-CM3. The 15-year sliding standard deviation of the TIO SST anomalies in the GFDL-CM3 is shown in Fig. 7. In r1i1p1, the standard deviation varies coincidently with the TSR during about 1870s to mid-1910s and mid-1950s to mid-1990s. The correlation coefficient between the sliding TSR and the sliding standard deviation of the TIO SST is 0.03 in r1i1p1, not reaching 90 % significance level. In r2i1p1, the standard deviation shows similar features throughout the whole period except after mid-1970s. The correlation coefficient is 0.69, far exceeding 99 % significance level. The relation between TIO SST variability and the TSR is not certain. The sliding TIO SST does not well match the TSR fluctuation from mid-19th century to the end of twentieth century in the two ensembles. The climatological SST of the TIO does not account for the TSR fluctuation on centurial timescale.

Figure 8 shows the correlation of the TIO SST index, as well as the SAH index, with the Indo-Pacific SST in GFDL-CM3 historical run during higher and lower TSR. It is based on the combination of r1i1p1 and r2i1p1. The higher (lower) relation cases are the highest (lowest) 30 correlation coefficient cases in the 21-sliding TSR, except that 31 cases are selected in the higher cases of r2i1p1 for the 30th equals the 31st in descent order. For short, the two cases are called “higher cases” and “lower cases”, respectively. The years of the two cases are list

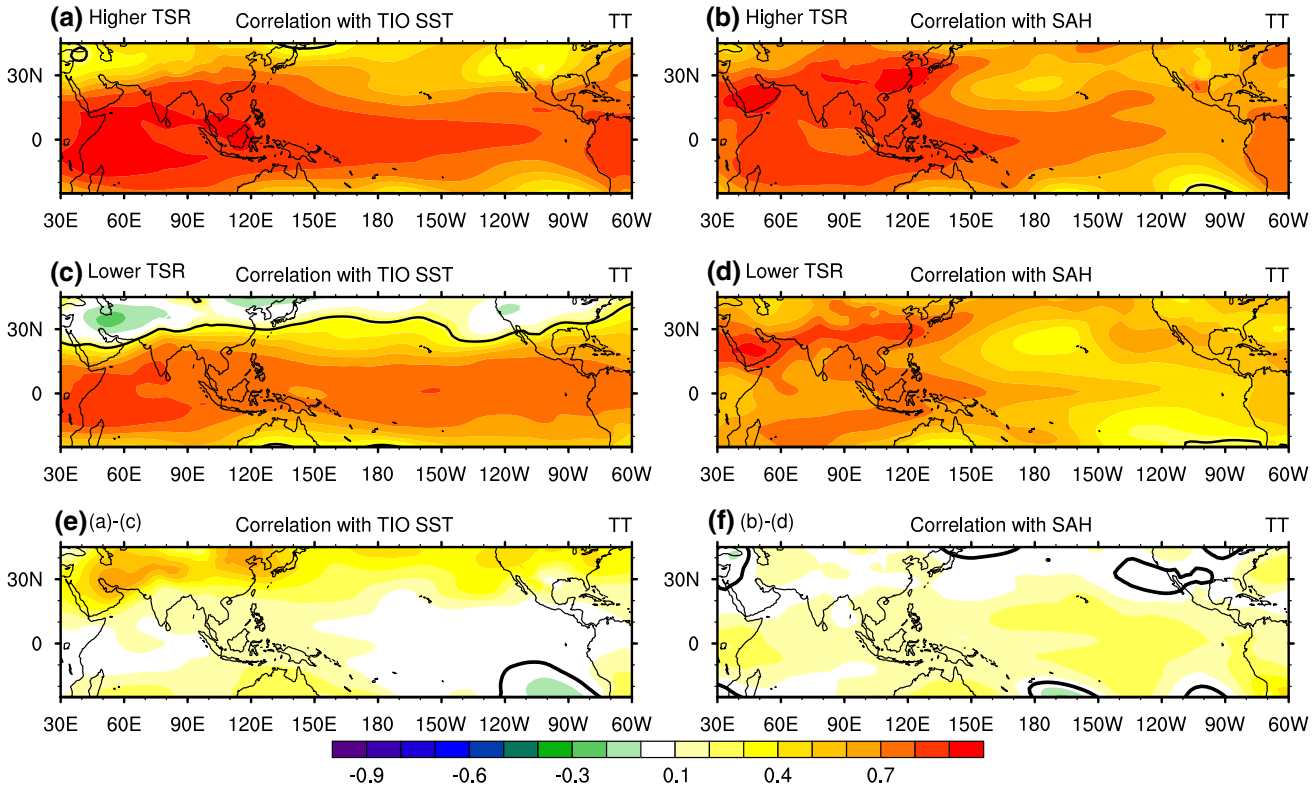

Fig. 10 The same as Fig. 8, except for JJA tropospheric temperature

in Table 2. A 9-year running average has been used to remove longer variation of the raw data. In the correlation results of the TIO SST index, when the TIO warms, IOBM exists in both cases. Compared with lower cases, the SST over the western (eastern) TIO is lower (higher) than that in higher cases. The regression of the TIO SST index against the TIO SST exhibits similar results (Fig. 9). In lower cases, when the TIO warms, the southwestern Indian Ocean show significant warming. It leads to the low-level northeasterly over the Arabian Sea (Du et al. 2009), which weakens the actual wind and favors the warming there (Fig. 9c). As suggested by the simulation results in Qu et al. (2014), excessive rainfall over south Asia may induce enhanced southwesterly monsoon flow. The anomalous northeasterly over the Arabia Sea in lower cases maybe contributed by the suppressed rainfall over the Indian subcontinent. The warming pattern indicates that the mechanism "significant SST anomalies within the warmpool when TIO warms" proposed by Qu and Huang (2012) does not explain the TSR in this period either. However, differences exist in the Pacific in the two cases. In the higher cases, significant warming exists in the northwestern Pacific. While, in the lower cases, the association of the western Pacific SST with the TIO SST is relatively weak (Fig. 8e). More accurately, the primary difference between the two cases is the western Pacific SST response. The sliding correlation between the TIO SST and western Pacific SST is calculated. The latter SST is defined as the area averaged SST in [20°S–20°N; 120°E–180°E] with latitudinal weight. It is shown in Fig. 7. The fluctuations are in good agreement with the sliding TSR. The correlation coefficients between the two are 0.55 in r1i1p1 and 0.77 in r2i1p1, both exceeding 99 % significance level. In the correlation results of the SAH index, the correlation pattern in higher cases is similar to the correlation results of the TIO SST index (Fig. 8b). During lower cases, significant warming in the northwestern Pacific is still associated with the SAH, but the association in equator is much weaker (Fig. 8d and f).

When the TIO basin warms, the concurrent Pacific warming anomalies heat the troposphere (Fig. 10), contributing to the tropospheric warming in the Tropics, including troposphere overlaying the TIO and the western Pacific. In higher cases, the warm western Pacific induces more significant tropospheric warming, spreading to the whole Tropics and strengthening the tropospheric warming near the TIO (Fig. 10a, c, e). It leads to the elevation of upper-troposphere geopotential, including the geopotential in the

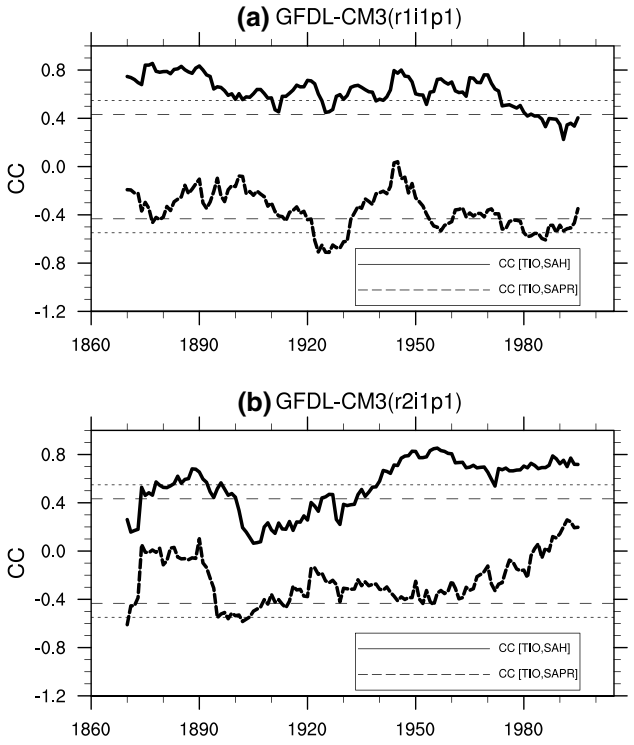

Fig. 11 The 21-year sliding correlation coefficient between the TIO SST and the SAH (*black solid line*) and correlation coefficient between the TIO SST and the precipitation over the Indian subcontinent [10°–30°N; 70°–95°E] SST (*black dash line*). The *long* (*short*) *thin dash line* means the correlation reaching 95 % (99 %) significance level. The results are based on GFDL-CM3 historical run. **a**, **b** The results of r1i1p1 and r2i1p1, respectively

south part of the SAH climatology position, and contributes to the enhancement of the SAH. It is evident in the difference of correlation of the TIO SST index between higher and lower cases (Fig. 10e). In the Tropics over the western Pacific and the maritime continents, the difference between the two cases is relatively larger; while, underlying is the relative larger SST difference (Fig. 8e).

In higher cases, the warmer troposphere over subtropical Asia greatly contributes to different response of SAH between the two cases (Fig. 10a, c, e). The difference may result from the less precipitation over the Indian subcontinent in lower cases. The anomalous rainfall excites anomalous upper-troposphere cyclone over the Tibet Plateau and Iran Plateau (Fig. 9d), leading to lower geopotential as well as less warmed troposphere. The 21-year sliding correlation of the TIO SST index with the Indian subcontinent precipitation [10°–30°N; 70°–95°E] (hereafter ISP) is shown in Fig. 11. The TIO SST–ISP correlation generally matches the TIO SST–SAH correlation. The correlation coefficient between the sliding TIO SST–ISP correlation and the 21-year sliding TSR is 0.49 in r1i1p1 and 0.43 in r2i1p1, both exceeding 99 % significance level. Thus, the ISP contributes to the difference of the SAH response in the two cases.

Regarding the correlation with the SAH index, the patterns in the two cases are similar except that the association of the SAH with TT over the Indo-Pacific and Asia continent is generally closer in higher cases (Fig. 10b, d, f).

Therefore, the outputs of GFDL-CM3 exhibit that, in the past about 150 years, when the TIO basin warms, the tropospheric warming over the TIO, as well as the intensified SAH, is the integrated effect of the TIO, Pacific SST and ISP; moreover, the TSR is modulated by the linkage of the western Pacific SST and the ISP to the TIO SST.

5 Influences under warmer climate

In warmer climate, the SAH is intensified due to hydrostatic equation; the center of the SAH in GFDL-CM3 moves little (Qu et al. 2014). Thus, the definition of the SAH index in historical is applicative to the warmer climate.

The TSR in RCP45 and RCP85 scenarios is generally higher than that in historical simulation, with more stable fluctuation (Fig. 12). In RCP45 scenario, the TSR generally displays a rising trend, sharing some feature with the TIO SST and global warming; while, in RCP85 run, the TSR does not show the same trend as the TIO SST, as well as global warming. It is not certain that the TSR is associated with the global warming. The western Pacific SST does not modulate the TSR in these scenarios. The correlation coefficient between the 21-year sliding TSR and the 21-year sliding TIO SST-western Pacific SST is -0.05 (0.15) in RCP45 (RCP85) run. While, the ISP still affects the TSR. The 21-sliding TIO SST–ISP with the 21-year sliding TSR is 0.39 in RCP45 run and 0.59 in RCP85 run, both exceeding 99 % significance level.

The SST and TT response patterns during higher and lower cases in RCP45 and RCP85 simulations are similar to those in historical simulation, except for the western Pacific regions (figures not shown). Figure 13 shows the regression of the normalized TIO SST index against precipitation in RCP45 and RCP85 runs. In RCP45 run, less precipitation exists over the Indian subcontinent as the TIO warms during both cases (Fig. 13a, c), but the anomalous rainfall is stronger during the lower cases (Fig. 13e). In RCP85 run, the IOBM associated ISP during the two cases are diverse. In higher cases, slight positive rainfall anomaly is found (Fig. 13b); while in lower cases, the rainfall is below average (Fig. 13d). In both the RCP45 and RCP85 runs, the stronger negative rainfall anomaly in lower cases contributes to the lower TSR.

Therefore, similar to the results in historical simulation, the less ISP when the TIO basin warms still works as a contributor to the lower TSR.

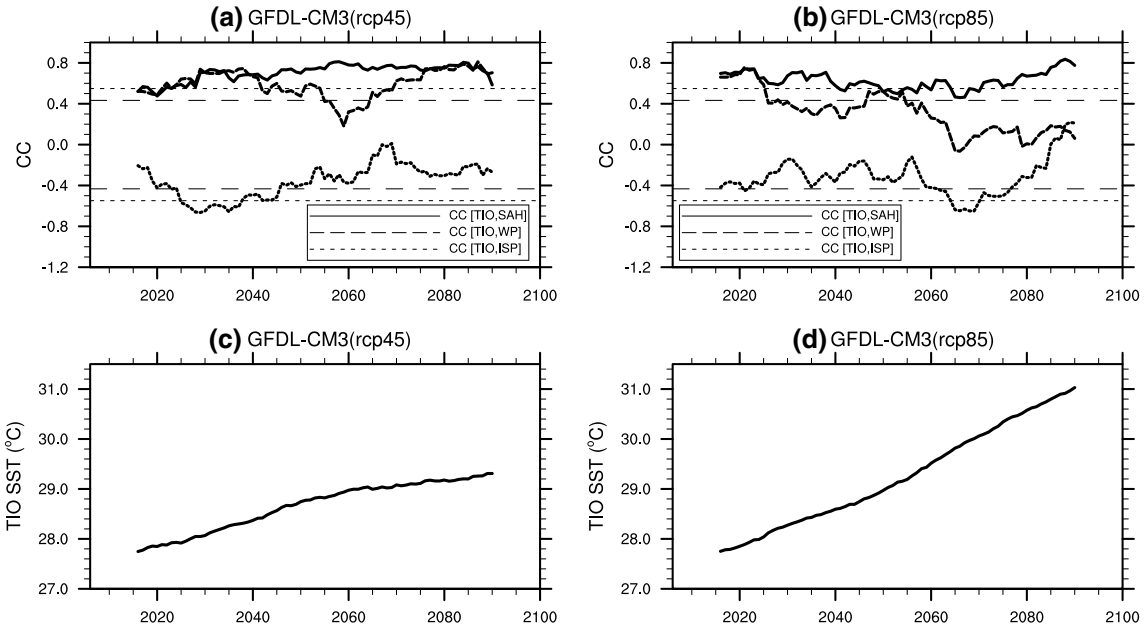

Fig. 12 **a**, **b** The 21-year sliding correlation coefficient between the TIO SST and the SAH (*black solid line*), correlation coefficient between the TIO SST and the western Pacific [20°S–20°N; 120°–180°E] SST (*black dash line*) and correlation coefficient between the TIO SST and the Indian subcontinent [10°–30°N; 70°–95°E] precipitation (*black dot line*). The 21-year sliding average of the TIO SST is shown in **c** and **d** in *blue line*. The *thin long* (*short*) *dash line* means the correlation reaching 95 % (99 %) significance level. The results are based on GFDL-CM3 RCP45 (**a**, **c**) and RCP85 (**b**, **d**) runs

6 Summary

Using 17 CMIP5 models, the influence of the TIO SST on the SAH is evaluated against the observational data (HadISST and NCEP–NCAR Reanalysis). First, the climatological pattern of the SAH is evaluated. The similarity and the standard deviation of the climatological pattern of the 100 hPa geopotential height over the domain of the SAH and the root-mean-square differences between simulations and observation are examined, the following models displays reasonable skills: CanESM2, CSIRO-Mk-3-6-0, GFDL-CM3, GFDL-ESM2G, IPSL-CM5A-LR, MIROC5, MPI-EMS-LR, MRI-CGCM3 and NorESM1-M. Second, the skill in the influences of the TIO SST on the SAH is examined in present-day climate (1980–2005). In observation, the IOBM follows El Niño in previous winter; in the following summer when the TIO basin warms, the TIO SST exerts influences on the surrounding regions. It excites Kelvin (Rossby) wave responses to the east (west). The overlaying upper troposphere features negative velocity potential. As the local troposphere warms, the SAH is enhanced. Among the CMIP5 models, only one, GFDL-CM3, displays the reasonable reproducibility of the influences.

By using GFDL-CM3, the decadal variability of the TSR from 1860 to 2005 is investigated based on the historical simulation. The TSR fluctuation acts like an internal variability in the past one and half century, not directly modulated by global warming. During that period, when the TIO basin warms, the gross features are similar when TSR is higher and lower: conspicuous warming exists in the TIO and the eastern/central Pacific and the whole Tropics are warmed. The differences between the higher and lower cases are: (1) the western Pacific warming is more apparent in the high cases; (2) the tropospheric warming is slightly northward over the Indian Ocean and the western Pacific in higher cases.

Two factors may influence the TSR fluctuation in the whole historical run: (1) the western Pacific SST. If the western Pacific warms in phase with the TIO, it may heat the atmosphere, contribute to the tropospheric warming over the TIO and strengthen the SAH, favoring the higher TSR; otherwise, the TSR is lower. (2) the ISP. During lower TSR, over the Indian subcontinent, if below-normal rainfall occurs as the TIO warms, it excites upper-troposphere cyclone over the Tibet Plateau and the Iran Plateau, causes negative geopotential and leads to lower TSR; otherwise, the TSR is higher.

Under RCP45 and RCP85 scenarios, the TSR is more stable and generally higher than that in historical simulations. The SST and TT features associated with the TIO warming during the higher and lower cases are similar to those in historical simulations except for the western Pacific region. The western Pacific SST do not modulate the TSR in these two scenarios; while, the ISP still affects

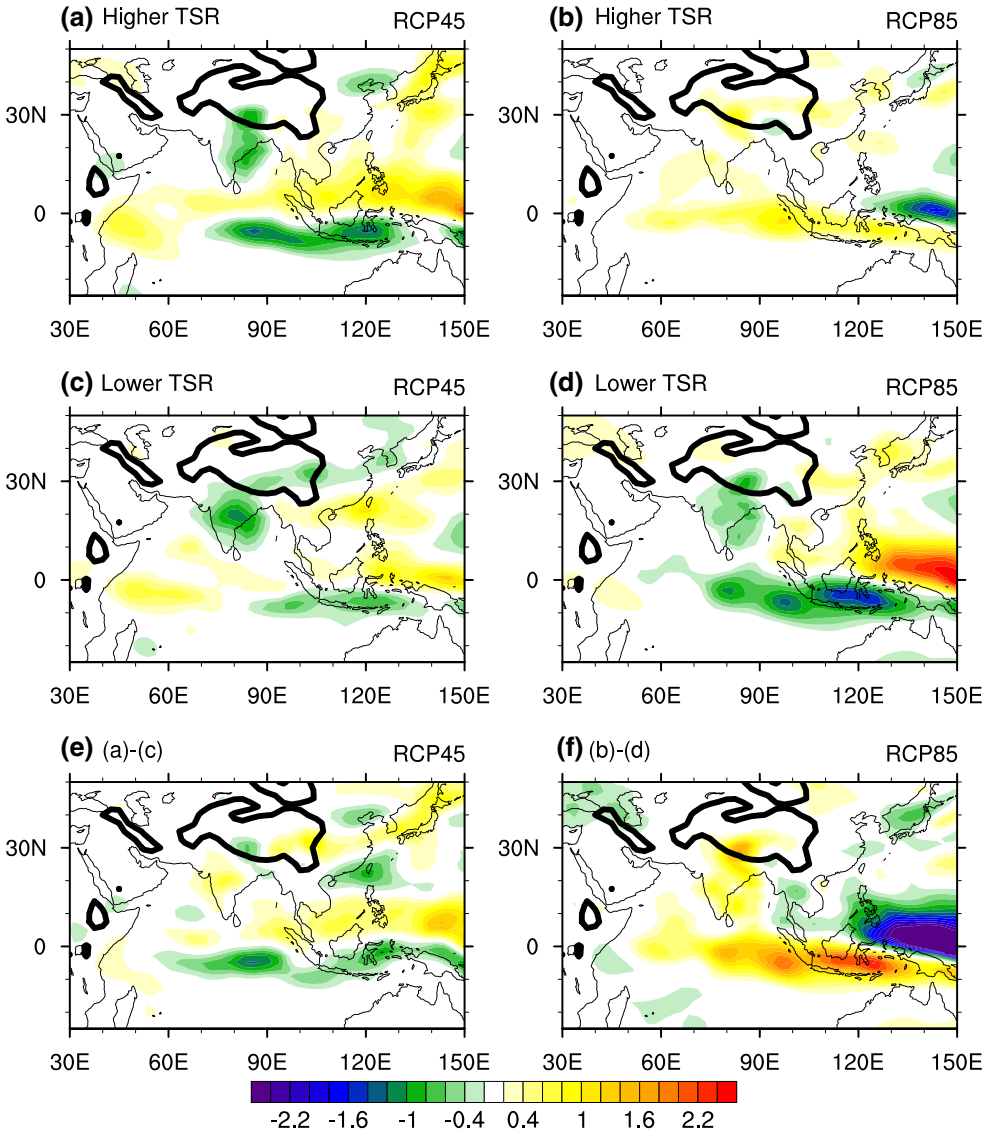

Fig. 13 The regression of the normalized TIO SST index in GFDL-CM3 RCP45 (**a**, **c**, **e**) and RCP85 (**b**, **d**, **f**) run against: precipitation (unit: mm/day). **a**, **b** The results of higher cases; **c**, **d** The results of lower cases. **e** The result of **a** minus **c**. **f** is the result of **b** minus **d**. *Thick contours* denote the elevation is 1,500 m. A 9-year running average has been used to remove longer variation of the raw data. Spatial 9-point smooth is performed for clarity

the TSR. In RCP45 run, negative rainfall anomaly is found over the Indian penisula in both higher and lower cases as the TIO warms, with stronger negative rainfall anomaly in lower cases. In RCP 85 run, the associated rainfall pattern is similar to that in historical simulation.

Acknowledgments We acknowledge the World Climate Research Programme's Working Group on Coupled Modelling, which is responsible for CMIP, and we thank the climate modeling groups (listed in Table 1 of this paper) for producing and making available their model output. For CMIP the U.S. Department of Energy's Program for Climate Model Diagnosis and Intercomparison provides coordinating support and led development of software infrastructure in partnership with the Global Organization for Earth System Science Portals." Besides, the authors wish to thank Prof. Renguang Wu and the reviewer for the insightful comments that lead to a significant improvement to the manuscript. The study was supported by National Basic Research Program of China (973 Program) 2012CB955604, Open Research Fund Program of Key Laboratory of Meteorological Disaster of Ministry of Education (Nanjing University of Information Science and Technology) Grant No. KLME1302 and National Natural Sciences Foundation of China (Grant Nos. 41205050, 91337105 and 41275083).

References

Annamalai H, Liu P, Xie SP (2005) Southwest Indian Ocean SST variability: its local effect and remote influence on Asian Monsoons. J Clim 18(20):4150–4167

Cai M (2005) Dynamical amplification of polar warming. Geophys Res Lett 32(22):L22710. doi:10.1029/2005GL024481

Chowdary JS, Xie SP, Luo J, Hafner J, Behera S, Masumoto Y, Yamagata T (2011) Predictability of Northwest Pacific climate during summer and the role of the tropical Indian Ocean. Clim Dyn 36:607–621

Chowdary J, Xie SP, Tokinaga H, Okumura YM, Kubota H, Johnson N, Zheng XT (2012) Interdecadal variations in ENSO teleconnection to the Indo-Western Pacific for 1870–2007. J Clim 25(5):1722–1744

Du Y, Xie SP (2008) Role of atmospheric adjustments in the tropical Indian Ocean warming during the 20th century in climate models. Geophys Res Lett 35(8):L08712. doi:10.1029/2008GL033631

Du Y, Xie SP, Huang G, Hu K (2009) Role of air–sea interaction in the longpersistence of El Niño–induced North Indian Ocean warming. J Clim 22(8):2023–2038

Du Y, Xie SP, Yang YL, Zheng XT, Liu L, Huang G (2013) Indian ocean variability in the CMIP5 multimodel ensemble: the basin mode. J Clim 26(18):7240–7266

Duan AM, Wu GX (2005) Role of the Tibetan Plateau thermal forcing in the summer climate patterns over subtropical Asia. Clim Dyn 24(7–8):793–807

Emanuel KA, Neelin JD, Bretherton CS (1994) On large-scale circulations in convecting atmospheres. Q J R Meteorol Soc 120(519):1111–1143

Emanuel KA, Neelin JD, Bretherton CS (1997) Reply to comments by Bjorn Stevens, David A. Randall, Xin Lin and Michael T. Montgomery on 'On large-scale circulations in convecting atmospheres'. Q J R Meteorol Soc 123(542):1779–1782

Hoskins BJ, Rodwell MJ (1995) A model of the Asian summer monsoon. Part I: the global scale. J Atmos Sci 52(9):1329–1340

Hu K, Huang G, Huang R (2011) The impact of tropical Indian Ocean variability on summer surface air temperature in China. J Clim 24(20):5365–5377

Hu K, Huang G, Qu X, Huang R (2012) The Impact of Indian Ocean variability on high temperature extremes across south of Yangtze River Valley in late summer. Adv Atmos Sci 29(1):91–100

Huang R, Sun F (1992) Impact of the tropical western Pacific on the East Asian summer monsoon. J Meteorol Soc Japan 70(1):243–256

Huang R, Wu Y (1989) The influence of ENSO on the summer climate change in China and its mechanism. Adv Atmos Sci 6(1):21–32

Huang R, Huang G, Ren B (1999) Advances and problems needed for further investigation in the studies of the East Asian summer monsoon. Chin J Atmos Sci 23(2):129–141

Huang G, Hu K, Xie SP (2010) Strengthening of tropical Indian Ocean teleconnection to the Northwest Pacific since the mid-1970s: an atmospheric GCM study. J Clim 23(19):5294–5304

Huang G, Qu X, Hu K (2011) The impact of the tropical Indian Ocean on the South Asian High in boreal summer. Adv Atmos Sci 28(2):421–432

Jiang XW, Li YQ, Yang S, Wu R (2011) Interannual and interdecadal variations of the South Asian and western Pacific subtropical highs and their realtionship with the Asian-Pacific summer climate. Meteorol Atmos Phys 113(4):171–180

Kalnay E, Kanamitsu M, Kistler R, Collins W, Deaven D, Gandin L, Iredell M, Saha S, White G, Woollen J (1996) The NCEP/NCAR 40-year reanalysis project. Bull Am Meteorol Soc 77(3):437–471

Klein SA, Soden BJ, Lau NC (1999) Remote sea surface temperature variations during ENSO: evidence for a tropical atmospheric bridge. J Climate 12(4):917–932

Li G, Xie SP (2014) Tropical biases in CMIP5 multimodel ensemble: the excessive equatorial pacific cold tongue and double ITCZ problems. J Clim 27:1765–1780

Li Q, Jiang JH, Wu DL, Read WG, Livesey NJ, Waters JW, Zhang Y, Wang B, Filipiak MJ, Davis CP (2005) Convective outflow of South Asian pollution: a global CTM simulation compared with EOS MLS observations. Geophys Res Lett 32:L14826. doi:10.1029/2005GL022762

Manabe S, Bryan K, Spelman MJ (1990) Transient response of a global ocean-atmosphere model to a doubling of atmospheric carbon dioxide. J Phys Oceanogr 20(5):722–749

Mason RB, Anderson CE (1963) The development and decay of the 100-MB summertime anticyclone over Southern Asia. Mon Weather Rev 91(1):3–12

Qu X, Huang G (2012) An enhanced influence of tropical Indian Ocean on the South Asia High after the late 1970s. J Clim 25(20):6930–6941

Qu X, Huang G, Hu K, Xie SP, Du Y, Zheng XT, Liu L (2014) Equatorward shift of the South Asian high in response to anthropogenic forcing. Theor Appl Climatol. doi:10.1007/s00704-014-1095-1

Rayner NA, Brohan P, Parker DE, Folland CK, Kennedy JJ, Vanicek M, Ansell TJ, Tett SFB (2006) Improved analyses of changes and uncertainties in sea surface temperature measured in situ since the mid-nineteenth century: the HadSST2 dataset. J Clim 19(3):446–469

Riahi K, Rao S, Krey V, Cho C, Chirkov V, Fischer G, Kindermann G, Nakicenovic N, Rafaj P (2011) RCP 8.5—a scenario of comparatively high greenhouse gas emissions. Clim Chang 109(1–2):33–57

Sutton RT, Dong B, Gregory JM (2007) Land/sea warming ratio in response to climate change: IPCC AR4 model results and comparison with observations. Geophys Res Lett 34(2):L02701. doi:10.1029/2006GL028164

Tao SY, Chen LX (1987) A review of recent research on the East Asian summer monsoon in China. In: Chang CP, Krishnamurti TN (eds) Monsoon Meteorology. Oxford University Press, USA, pp 60–92

Tao S, Zhu F (1964) The variation of 100mb circulation over South Asia in summer and its association with march and withdraw of West Pacific Subtropical High. Acta Meteorol Sin 34(4):385–395

Thomson AM, Calvin KV, Smith SJ, Kyle GP, Volke A, Patel P, Delgado-Arias S, Bond-Lamberty B, Wise MA, Clarke LE (2011) RCP4. 5: a pathway for stabilization of radiative forcing by 2100. Clim Chang 109(1):77–94

Wu R, Chen L (1998) Decadal variation of summer rainfall in the yangtzehuaihe river valley and its relationship to atmospheric circulation anomalies over East Asia and western north pacific. Adv Atmos Sci 15(4):510–522

Xie SP, Annamalai H, Schott FA, McCreary JP (2002) Structure and mechanisms of South Indian Ocean climate variability. J Clim 15(8):864–878

Xie SP, Hu K, Hafner J, Tokinaga H, Du Y, Huang G, Sampe T (2009) Indian Ocean capacitor effect on Indo-Western Pacific climate during the summer following El Niño. J Clim 22(3):730–747

Xie SP, Deser C, Vecchi GA, Ma J, Teng H, Wittenberg AT (2010a) Global warming pattern formation: sea surface temperature and rainfall. J Climate 23(4):966–986

Xie SP, Du Y, Huang G, Zheng X-T, Tokinaga H, Hu K, Liu Q (2010b) Decadal shift in El Niño influences on Indo-western Pacific and East Asian climate in the 1970s. J Clim 23(12):3352–3368

Yang J, Liu Q, Xie SP, Liu Z, Wu L (2007) Impact of the Indian Ocean SST basin mode on the Asian summer monsoon. Geophys Res Lett 34(2):L02708. doi:10.1029/2006GL028571

Zhang Q, Qian Y, Zhang X (2000) Interannual and interdecadal variations of the South Asia High. Chin J Atmos Sci 24(1):67–78

Zhang P, Yang S, Kousky VE (2005) South Asian High and Asian-Pacific-American climate teleconnection. Adv Atmos Sci 22(6):915–923

Zhao P, Zhu Y, Zhang R (2007) An Asian-Pacific teleconnection in summer tropospheric temperature and associated Asian climate variability. Clim Dyn 29(2):293–303

Zhao P, Zhang X, Li Y, Chen J (2009) Remotely modulated tropical-North Pacific ocean–atmosphere interactions by the South Asian high. Atmos Res 94(1):45–60

Zhou N, Yu Y, Qian Y (2006) Simulation fo the 100-hPa South Asian High and precipitation over East Asia with IPCC coupled GCMS. Adv Atmos Sci 23(3):375–390

Zhou N, Yu Y, Qian Y (2009) Bimodality of the South Asia High simulated by coupled models. Adv Atmos Sci 26(6):1226–1234